Indirect-to-direct gap transition in strained and unstrained Sn_xGe_{1-x} alloys

C. Eckhardt, K. Hummer,[*] and G. Kresse

University of Vienna, Faculty of Physics and Center for Computational Materials Sciences, Sensengasse 8/12, 1090 Vienna, Austria

(Received 20 December 2013; revised manuscript received 6 March 2014; published 9 April 2014)

The transition from an indirect to a direct gap semiconductor in unstrained as well as compressively and tensile strained Sn_xGe_{1-x} alloys is investigated as a function of the Sn content $0 \leq x \leq 1$ by means of both a very accurate supercell approach and the more approximate virtual crystal approximation (VCA). In the local density approximation we calculate the bowing parameter of the lattice constant of unstrained Sn_xGe_{1-x} alloys. Provided that pseudopotentials suitable for the VCA are used, the random supercell and VCA approaches yield consistent bowing parameters for the lattice constant of −0.21 and −0.28 Å, respectively, in the entire Sn concentration range. The band structures and energy gaps are calculated using the modified Becke-Johnson potential, which, for Ge, yields a one-electron band gap in very good agreement with experimental data. The crossover from an indirect to a direct gap semiconducting alloy is determined at about 4.5% Sn in unstrained Sn_xGe_{1-x}. When Sn_xGe_{1-x} is grown commensurately and thus strained on Ge(100), a transition to a direct gap is also observed but at Sn concentrations of about 10%. We finally predict the direct and indirect band gaps as a function of the in-plane lattice constant and Sn concentration for Sn_xGe_{1-x} alloys grown on (100) substrates.

DOI: 10.1103/PhysRevB.89.165201 PACS number(s): 71.22.+i, 71.20.Mq, 71.23.An

I. INTRODUCTION

One fundamental problem of the well-established Si and Si/Ge semiconductor technology is the indirect nature of the fundamental band gap resulting in inefficient absorption and emission of light. For example, efficient light-emitting diodes require a direct semiconductor as active material. Another aspect that is important for optoelectronic applications is the magnitude of the semiconductor band gap, which determines the wavelength of the photoabsorption/photoemission. For future applications, materials with a tunable band gap are desired. To overcome the limitations stemming from the indirect band gap in Si/Ge and to benefit from good integration and compatibility to Si-based technology, mainly two strategies have been considered. The first involves growing heterostructures of group IV semiconductors, where the lattice mismatch induces strain and thus changes the magnitude and possibly the nature of the band gap [1]. The most prominent example is the Si/Ge materials system [2]. A second route is the alloying of Ge with other elements, for instance Sn [3–6]. The combination of these two routes is possibly the most promising approach [7], often also enabling a widely tunable band gap.

Using strain, direct band gaps were achieved in single-crystal Ge nanowires [1]. At ambient conditions, elemental Ge exhibits an indirect (direct) band gap of 0.66 (0.80) eV [8]. The energy difference between the absolute conduction-band minimum (CBM) located at the L point in the Brillouin zone (L_6 symmetry) and the local CBM at the Γ point (Γ_7 symmetry) is 140 meV. It has been shown by Zhang *et al.* [1] that this energy separation can be reduced in germanium nanowires by uniaxial tensile strain along the [111] direction leading to direct gap Ge nanowires. Another practical route to introduce tensile strain is the epitaxial growth of Ge on substrates with larger lattice constants such as Sn containing group IV alloys or III-V semiconductors [7].

In this work, we concentrate on the Sn_xGe_{1-x} alloy, which is among the most promising candidates in order to obtain a direct band gap group IV semiconductor. Sn_xGe_{1-x} alloys can be either used as substrates or as the active material. Below 13 °C Sn exists in the α-Sn (gray tin) phase with diamond structure, but undergoes a phase transition to β-Sn (white tin) above this temperature. In the present work, we assume that the aforementioned phase transition does not destabilize the zinc-blende alloy. In contrast to Ge, α-Sn is a zero-gap semiconductor. At the Γ point the antibonding s-like conduction-band state (Γ_7 symmetry) drops below the p-type valence band level (Γ_8 symmetry), resulting in a negative direct band gap of −0.41 eV [8]. Assuming a simple linear approximation of the Sn_xGe_{1-x} alloy band structure from its constituents according to Vegard's rule [9], one would propose the crossover to a direct gap semiconductor at a Sn concentration of $x = 0.22$. The pioneering work of He and Atwater [3]—optical absorption experiments with zinc-blende Sn_xGe_{1-x} alloy films of different Sn concentrations—showed a strong interband transition with a crossover to a direct gap of $0.35 < \Delta E_\Gamma < 0.80$ eV for $0 < x < 0.15$. This observation was confirmed independently experimentally by D'Costa *et al.* [5] and Pérez Ladrón de Guevara [10]. According to the positive Sn-concentration-dependent bowing parameter of the lattice constant as well as the energy gap, a much lower crossover concentration close to $x = 0.06$ [6] was found by recent *ab initio* calculations [11].

Current research on direct gap Sn_xGe_{1-x} alloy films [6,11] targets at technical aspects of its realization. An important issue is the effect of strain on the electronic properties of Sn_xGe_{1-x} studied in detail by Fischetti and Laux [2] and very recently by Gupta *et al.* [12], both using the nonlocal empirical pseudopotential method (NL-EPM). In the present work we investigate the electronic properties of compressively and tensile-strained Sn_xGe_{1-x} alloys using more accurate *ab initio* (parameter-free) methods instead of the EPM. We concentrate on the (100) growth direction (basal plane), since most commercial Ge wavers possess this orientation. To model the alloys two widely adopted methods are used and

[*]Corresponding author: kerstin.hummer@univie.ac.at

 ©2014 American Physical Society

compared. The more approximate method is the virtual crystal approximation (VCA). In this approximation, virtual atoms are introduced that represent a properly weighted average of the Ge and Sn atoms. This is obviously an approximation. The more accurate approach is based on the use of large random superstructures, here containing more than 200 atoms. This should represent the true experimental situation very reliably. The comparison between the more approximate VCA and the accurate supercell approach is interesting in itself and of relevance beyond the particular materials system considered here. The VCA is computationally efficient but rather approximate, whereas the supercell approach is accurate but computationally demanding. To what extent do the results of these two approaches agree?

The paper is organized as follows. After summarizing the methodologies applied in the calculations in Sec. II, the results are discussed in Sec. III. As elaborated above, structure optimization was performed within the VCA and using large supercells. In both cases, the local density approximation was applied for relaxation. Deviations of the alloy lattice parameters from Vegard's rule are investigated. The main part of Sec. III is devoted to the electronic properties of the alloy, in particular the indirect-to-direct gap transition and Sn-dependent band bowing parameters. In this part a special density functional is applied. This density functional yields accurate band gaps for Ge in excellent agreement with experiment.

II. METHODS OF CALCULATION

A. Basis sets and exchange correlation potentials

The density functional theory [13,14] calculations were performed using the Vienna *ab initio* simulation package (VASP) [15] utilizing the projector augmented plane-wave (PAW) method [16] to describe the core-valence interaction. For structure optimizations, the exchange correlation (XC) potential was treated within the local density approximation (LDA) [17]. This was motivated by the observation that semilocal XC functionals, i.e., PBE [18] or PBEsol [19], yield significantly too large lattice constants for Ge and Sn. Those large lattice constants then cause a wrong band order and inaccurate fundamental gaps [20]. The LDA underestimates the volume, but only very slightly. All calculations were performed with PAW potentials treating only the Ge(Sn) *4(5)s* and *4(5)p* states as valence states. As described below, the Ge/Sn semicore *d* states were treated as core electrons in all calculations. Unfreezing them showed little change in the results.

For cell shape relaxations, the energy cutoff for the plane-wave basis set was set to 300 eV for the small unit cells. With this large cutoff the stress tensor is essentially free of the Pulay stress error, allowing for straightforward volume relaxations. For the supercell calculations, the cutoff was reduced to 148 eV, but the stress tensor was then corrected for the errors introduced by the finite basis set (Pulay stress).

All band structure calculations were performed using a smaller cutoff of 148 eV. In order to improve the description of the band structure, the modified Becke-Johnson LDA (MBJ-LDA) potential developed by Tran and Blaha [21] was applied. This semilocal XC potential combines the modified Becke-Johnson exchange potential with LDA correlation and provides a good description of fundamental band gaps at comparatively low computational costs. If properly tuned, this XC potential can yield excellent agreement with experimental band structures [21,22]. MBJ-LDA calculations are suitable for the large supercells investigated in this work, where hybrid functionals or GW calculations are simply too time-consuming. This, however, also implies that the present calculations carry some kind of empiricism. Since we have tuned the single parameter in MBJ carefully to match the available experimental data, we expect that the predictions are fairly accurate. In general, the present approach is expected to possess higher predictive power than semiempirical pseudopotential calculations; in particular, only a single parameter needs to be adjusted to fit the band structure of bulk Ge.

B. Structure optimization, virtual crystal approximation, and PAW potentials

In previous work, the Sn concentration was limited to $x > 6\%$ by the rather small supercells: Yin, Gong, Wei [11] used 64 atom cells, and Ventura *et al.* [23] applied 8, 16, and 64 atom supercells. In the present work, this issue was addressed by employing $3 \times 3 \times 3$ supercells of the conventional cubic cell of the zinc-blende structure. This corresponds to $216 = 3 \times 3 \times 3 \times 8$ atoms, and the smallest possible Sn concentration is thus about 0.5%. Tests using $4 \times 4 \times 4$ supercells containing 512 atoms did not change the results, but required significantly more computer time. In the first step, Sn_xGe_{1-x} alloy structures with Sn concentrations between $0 \leq x \leq 1$, with $x = \{0, 2, 5, 10, 20, 25, 30, 40, 50, 75, 100\}\%$, were investigated. The lattice constants were initially interpolated using Vegard's rule [9],

$$a_{Sn_xGe_{1-x}} = x a_{Sn} + (1 - x) a_{Ge}. \quad (1)$$

It was already pointed out that the unit cell volumes of the Sn_xGe_{1-x} alloys deviate from this simple linear approximation [5]. Hence, these structures were subjected to an optimization of the lattice constants utilizing the VCA [24]. For the VCA calculations, special PAW potentials with identical core radii for the Ge and Sn atoms were generated. Specifically, the core radii for the *s* and *p* partial waves were set to 2.3 and 2.5 a.u., respectively. The local potential was constructed by pseudizing the Sn all-electron potential below a core radius of 2.0 a.u. For Ge the same local pseudopotential was chosen between the atomic core and 1.4 a.u.; beyond this radius the all-electron potential of Ge was used as local potential. This procedure guarantees that the pseudoorbitals of Sn and Ge possess a very similar shape inside the atomic spheres. A common local potential makes the nonlocal projectors similar and significantly improves the description within the VCA.

The more approximate alloy calculations are performed using the VCA, as described by Bellaiche and Vanderbilt [24]. For a specific concentration of Sn_xGe_{1-x}, this is achieved by weighting the PAW potentials of Sn by a factor x, and the PAW potentials of Ge by a factor *1–x*. An important comment is in place here. We also tried to generate VCA potentials with the *d* electrons in the valence. However, this

turned out to be impossible, since the Ge 3d electrons possess a very different spatial distribution compared to the Sn 4d electrons. If the 3d and 4d electrons are treated as valence electrons in the VCA, the electronic structure code needs to find a compromise between the spatial distribution of the 3d and 4d orbitals. This causes unreliable results and large errors in the mean energy position of the d levels; they are generally well above the mean position of the supercell 3d and 4d orbitals. Quite generally, the VCA is only reliable if the considered valence orbitals are spatially reasonably similar. For instance, after pseudization the Ge 4s and Sn 5s pseudoorbitals, and the Ge 4p and Sn 5p pseudoorbitals are rather similar inside the pseudization sphere. To achieve this similarity requires considerable care, when constructing VCA potentials, and the standard PAW potentials distributed with the VASP code are generally not suitable for VCA calculations.

In the VCA calculations, the volume was optimized automatically using a large cutoff (300 eV). Alternatively, the volume was varied in the range of 0.9–1.1 V_0, and the self-consistently converged total energies fitted to a Murnaghan equation of state (EOS) [25]. This procedure can be safely adopted even at low-energy cutoffs (148 eV) and yields identical results to the automatic relaxations at large plane-wave cutoff energies. For pure Ge and Sn, the present potentials yield an optimized LDA lattice constant of $a_{\mathrm{Ge}} = 5.644$ Å and $a_{\mathrm{Sn}} = 6.481$ Å, which is in good agreement with the experimental values of 5.658 Å [8] and 6.49 Å [8] for Ge and Sn, respectively.

The more accurate alloy calculations were performed using actual random supercells. From the VCA primitive unit cells obtained in the first step, $3 \times 3 \times 3$ supercells were constructed corresponding to *effective* Sn concentrations of $x = \{0, 1.89, 4.85, 9.72, 19.9, 25, 29.6, 39.8, 50, 75, 100\}\%$. In the supercells, only an integer number of Ge atoms can be replaced by Sn atoms, resulting in the specified effective Sn concentrations x. For each $\mathrm{Sn}_x\mathrm{Ge}_{1-x}$ supercell, ten different structures with Sn and Ge atoms randomly distributed on the lattice positions were created. In order to guarantee completely unstrained structures, each random structure was optimized with respect to the atomic positions for a range of volumes between 0.9 V_0 and 1.1 V_0, as already described above for the primitive VCA cell. The atomic positions were optimized by minimization of the forces acting on the atoms. Typically, the forces were converged to better than 0.01 eV/Å. The optimized volume was then determined by a Murnaghan's EOS fit.

With the aim to better match experimental conditions, i.e., alloy structures grown by molecular beam epitaxy (MBE) on the Ge (100) substrates, the modeling was also performed with strained alloy structures. In this case, the in-plane lattice constants a and b (perpendicular to the growth direction) were set to the LDA optimized value for Ge $a = b = 5.644$ Å, whereas the lattice parameter parallel to the growth direction (c parameter) was optimized to yield a minimal energy. This was achieved again by a fit to Murnaghan's EOS, but now only the lattice parameter c was optimized. This procedure leads to laterally, compressively strained structures corresponding to epitaxial growth of the $\mathrm{Sn}_x\mathrm{Ge}_{1-x}$ alloy on the Ge (100) substrate.

C. Brillouin sampling and zone folding

For the structure optimizations using the VCA in the zinc-blende cell, Γ-centered k meshes with $16 \times 16 \times 16$ k points were used to carry out the Brillouin zone integration. For all supercell calculations, however, only the Γ point was considered in the structure optimizations with some calculations double checked using $2 \times 2 \times 2$ k points.

The MBJ supercell band structure calculations were performed with the Γ point and additional k points along high-symmetry directions. To determine the band structure in the primitive cell, a "simple" backfolding scheme described in the following is applied. Orbitals with eigenenergies $\varepsilon_{n\mathbf{K}}$ in the supercell are linear combinations of plane waves

$$\varphi_{n\mathbf{K}}(\mathbf{r}) = \sum_{\mathbf{G}} C_{n,\mathbf{G}+\mathbf{K}} e^{i(\mathbf{G}+\mathbf{K})\mathbf{r}}, \quad (2)$$

where the vectors $\mathbf{G}$ are reciprocal lattice vectors of the supercell, and $\mathbf{K}$ is a Brillouin zone vector in the supercell. With the zone folding relation, $\mathbf{K}$ is related to a wave vector in the primitive cell $\mathbf{k}$ by the relation $\mathbf{G} + \mathbf{K} = \mathbf{g} + \mathbf{k}$ (see, e.g., Ref. [26]). One can exactly rewrite Eq. (2) as

$$\varphi_{n\mathbf{K}}(\mathbf{r}) = \sum_{\mathbf{k}} \sum_{\mathbf{g}} C_{n,\mathbf{g}+\mathbf{k}} e^{i(\mathbf{g}+\mathbf{k})\mathbf{r}}, \quad (3)$$

where $\mathbf{g}$ is a reciprocal lattice vector of the primitive cell and $\mathbf{k}$ is a k point in the first Brillouin zone of the original primitive cell, in the present case the zinc-blende structure with two atoms. The norm of the orbital can then be rewritten as

$$\langle \varphi_{n\mathbf{K}} | \varphi_{n\mathbf{K}} \rangle = \sum_{\mathbf{k}} \sum_{\mathbf{g}} |C_{n,\mathbf{g}+\mathbf{k}}|^2 = \sum_{\mathbf{k}} w_{n\mathbf{K},\mathbf{k}}, \quad (4)$$

where

$$w_{n\mathbf{K},\mathbf{k}} = \sum_{\mathbf{g}} |C_{n,\mathbf{g}+\mathbf{k}}|^2, \quad (5)$$

This simple procedure makes it possible to assign the original eigenvalue $\varepsilon_{n\mathbf{K}}$ to k points in the original primitive cell and represents a simplification of the effective band structure (EBS) method proposed by Popescu and Zunger in Refs. [26,27]. In that work, a spectral weight is derived from the supercell eigenvectors by projecting them onto a set of eigenfunctions in the primitive cell. The present procedure is simpler and does not require the calculation of the eigenfunctions in the primitive cell. Our approach can be derived from the approach of Popescu and Zunger realizing that the eigenstates of the primitive cell form a complete Hilbert space at each k point. Using this exact identity our $w_{n\mathbf{K},\mathbf{k}}$ can be identified as $P_{\mathbf{K}n}(\mathbf{k})$ in Eq. (8) of Ref. [27]. The only "drawback" of the present approach is that some states and eigenvalues might be assigned to multiple k points; however, this is also the case for the method of Popescu and Zunger. For instance, orbitals from the three X points in the original primitive cell (X, Y, Z) have all the same eigenvalues, and the three states mix in the supercell calculation. It is, therefore, usually not possible to uniquely assign the orbital in the supercell to the X, the Y, or the Z point. For the present purpose, this is of little consequence, since we only attempt to fold the original states back to the irreducible wedge of the zinc-blende primitive cell, and hence the distinction between X, Y, and Z does

not matter: One simply needs to sum the weights $w_{n\mathbf{K},\mathbf{k}}$ over k points that are symmetry equivalent in the original primitive cell. More problematic is that the conduction-band states have very similar energies at L and Γ, in particular, at concentrations where the gap changes from indirect Γ-L to a direct Γ-Γ transition. In this case, strong hybridization between the original Γ and L conduction-band minima can occur, and the assignment becomes ambiguous. In the present case, this is avoided by using $3 \times 3 \times 3$ supercells, so that the original L point is mapped onto the distinct point (0.5, 0.5, 0.5) $2\pi/a$ in the supercell. Thus, states originating from the L and the Γ points can be distinguished without ambiguity.

D. MBJ calculations of alloy band structures

The VASP implementation of the modified Becke-Johnson potential either determines the parameter c-MBJ self-consistently or allows calculations with a fixed parameter [22]. The latter approach has been chosen for the present study and the optimal c-MBJ parameter was determined by calculating the band gap of pure germanium and comparing it to the experimental value. The best match was obtained with c-MBJ = 1.2. This parameter has been kept constant throughout all alloy calculations. This is the only parameter used in the present calculations; otherwise, the calculations are entirely *ab initio*.

The theoretical direct gaps calculated using the MBJLDA potential (c-MBJ = 1.2) at the lattice constant optimized within LDA (a_{Ge} = 5.644 Å and a_{Sn} = 6.481 Å) are $E_g(\mathrm{Ge})$ = 0.97 eV and $E_g(\mathrm{Sn}) = -0.12$ eV, with an indirect fundamental minimum Ge gap of 0.82 eV. Including SOC in the MBJLDA calculations reduces the direct gap to $E_g(\mathrm{Ge})$ = 0.87 eV and $E_g(\mathrm{Sn}) = -0.24$ eV and the indirect gap in Ge to 0.72 eV.

These values agree well with the measured direct and indirect low-temperature gaps of 0.89 and 0.74 eV, respectively [8]. Specifically the difference between the direct and indirect gap is in excellent agreement with experiment, which is particularly relevant to the present study.

E. Calculations of the bowing parameter

Many binary semiconductor alloys A_xB_{1-x} have a nonlinear dependence of their physical properties, e.g., lattice constants or band gaps, as a function of the alloy composition x. This is commonly described by a second-order polynomial of the form

$$a_{\mathrm{Sn}_x\mathrm{Ge}_{1-x}} = x a_{\mathrm{Sn}} + (1-x)a_{\mathrm{Ge}} - bx(1-x). \quad (6)$$

Here b denotes the bowing parameter. When the lattice constant a is replaced by the direct band gap E_g, b is also called *optical bowing* or *optical bowing parameter* b_g.

III. RESULTS AND DISCUSSION

When alloy samples are experimentally prepared, the distribution of the Sn atoms in the Ge matrix is often governed by thermodynamics. The Sn atoms can be randomly distributed, form a regular superstructure, or coalesce into a larger cluster. The question of whether the Sn atoms form clusters in the Ge matrix has been investigated by Ventura *et al*. [23], who concluded that homogeneous SnGe alloys

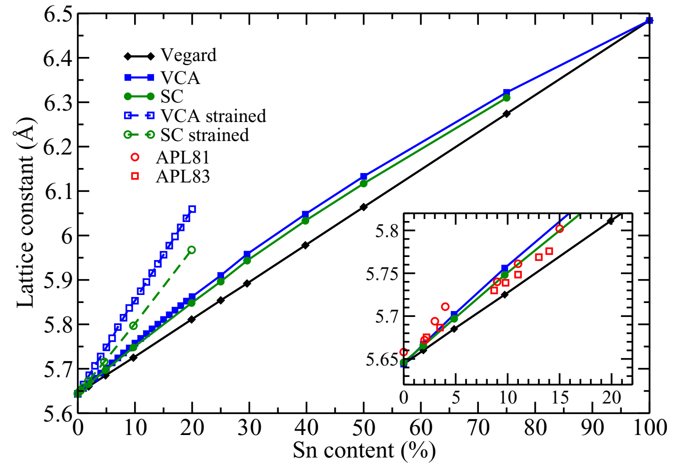

FIG. 1. (Color online) $\mathrm{Sn}_x\mathrm{Ge}_{1-x}$ alloy lattice constant (Å) as function of the Sn content (%). Volume and atomic position relaxed random supercells (green circles), VCA calculations (blue squares), and laterally biaxial strained supercells on Ge (100) are compared to the linear dependence corresponding to Vegard's rule (black line). APL81 and APL83 indicate the results of Refs. [6] and [28], respectively.

with Sn atoms substitutionally incorporated in the Ge matrix are energetically preferred in the lower concentration range, whereas metallic Sn clusters resulting in inhomogeneous defect structures are preferred at high Sn concentrations. Here we have considered only fully random structures. Although this might not be the energetically preferred arrangement, we believe that such random structures are generated under the growth conditions of MBE and thus provide a valid model for the experimental situation. Moreover, random structures are most appropriate for investigating the electronic properties of random alloys within the concept of band theory. Also by avoiding any disorder-order phase transition, we can expect smooth variations of the evaluated properties as a function of the Sn concentration, so that sensible bowing parameters can be determined.

The results of the optimization (lattice constants) of the more approximate VCA (blue line) and the random supercells (green line) for each Sn content are compared to the lattice constants obtained from Vegard's rule in Fig. 1. Again we emphasize that the results for the random supercells are the reference, to which the VCA calculations can and should be compared. As expected from the large lattice mismatch and confirmed by previous work [5,6,29], the optimized lattice constants of the alloy clearly deviate from a linear dependence on x (Vegard's rule). Hence, structures generated using Vegard's rule without any optimization are not suitable for describing the structural and electronic properties of the $\mathrm{Sn}_x\mathrm{Ge}_{1-x}$ alloys. The deviation from Vegard's rule is positive, resulting in a negative bowing parameter, which is opposite to the observations for $\mathrm{Si}_x\mathrm{Ge}_{1-x}$ alloys [5,6]. Compared to the supercell approach, the VCA yields a quite accurate description of the lattice parameters for the investigated compositions, although upon closer inspection the deviation from Vegard's rule is overestimated by about 25% for the VCA. The good match of the VCA and supercell results relies on the

particular VCA PAW potentials employed here and should not be taken for granted, as discussed in the Methods section. The bowing parameter b of the lattice constant with respect to x evaluated from a quadratic fit of the supercell and VCA data for $0 \leq x \leq 1$ is −0.21 and −0.28 Å, respectively. As already mentioned, the VCA overestimates the bowing by about 25%. Our values are in reasonable agreement with D'Costa *et al.*, who deduced -0.17 Å $< b < 0$ Å from high-resolution x-ray diffraction of Sn_xGe_{1-x} samples with $x \leq 0.2$ [5]. In contrast, Chibane and Ferhat obtained a significantly larger bowing coefficient of the lattice constant, i.e., −0.65 Å from VCA calculations of Sn_xGe_{1-x} alloys with $0 \leq x \leq 0.19$ [29]. In order to understand the discrepancies, the quadratic fit of the present data was also restricted to $x \leq 0.2$ for the VCA. In this case, a larger $b = -0.45$ Å is obtained. Thus, the fit is somewhat dependent on the considered fitting range; however, the increase from −0.28 to −0.45 Å is not sufficient to fully explain the discrepancy to the results of Chibane and Ferhat. We believe that the present results are more accurate, since the present approach is less empirical, and since the present VCA are evaluated by reference supercell calculations.

The structure optimization of laterally strained supercells with the lattice constants a and b fixed to the Ge lattice constant (5.644 Å) yield, as expected, a much larger increase of the lattice constant in the c direction. If the volume increase were similar to the isotropic case (perfectly elastic), one would expect that the increase of the lattice constant in the c direction were three times larger than for relaxation in all three directions. However, the increase of the lattice constant in the strained case is only about twice as large as for the isotropic case. The calculated Poisson's ratio is 0.4, which agrees well with the observed behavior. As before, the VCA overestimates the increase in the lattice constant c by about 25%.

A. Alloy band structures as function of the composition

The alloy band structures obtained by the unfolding procedure of the supercell, as described in Sec. II B, are depicted in Figs. 2(a)–2(c) for $x = 1.89\%$ (a), $x = 4.85\%$ (b), and $x = 9.72\%$ (c) as discrete data. The distance between the two horizontal lines above and below each data point indicates the standard deviation calculated from the ten supercells. Note that the deviations are only in the energy (y axis) and not in the k point (x axis), but since the deviations are so small, often only a single horizontal line is discernible. The VCA band structures are shown by continuous lines. In these graphs, the valence bands formed by semiconductor s states (gray line) and the p states, as well as the lowest conduction band comprised by p states (red line) are shown from the zone center $\Gamma = (0, 0, 0)$ towards $L = (0.5, 0.5, 0.5)\ 2\pi/a$. The two uppermost valence bands (green line) with a total angular momentum $J = 3/2$, i.e., the *heavy hole* (with z component $Jz = \pm 3/2$) and the *light hole* ($Jz = \pm 1/2$), are degenerate along Γ-L, since spin-orbit coupling (SOC) was not taken into account in the calculations. The *third* band with $J = 1/2$ (turquoise line), usually referred to as the *split-off band*, is also degenerate with the other two bands at the Γ point due to neglect of SOC. Since the common nomenclature does not fully apply here, the uppermost valence band (twofold degenerate, green) is denoted with VB1, and the lower one (turquoise) with VB2 throughout the paper.

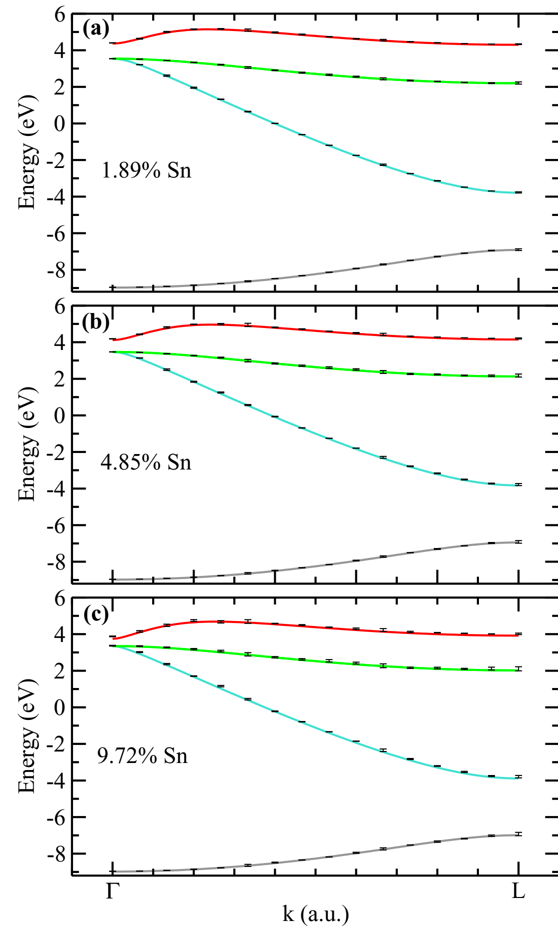

FIG. 2. (Color online) Sn_xGe_{1-x} band structures of unstrained alloys obtained by averaging over ten structurally relaxed random supercells with a Sn content of (a) $x = 1.89\%$, (b) $x = 4.85\%$, and (c) $x = 9.72\%$. The upper and lower lines indicate the standard deviation evaluated from the ten considered models. The lines indicate the calculated VCA band structures. The lowest conduction band is shown in red, whereas the topmost four valence bands are indicated in green (twofold degenerate p band, *heavy hole* and *light hole*, here VB1), turquoise (*split-off* p band, here VB2), and gray (s character) lines. SOC was not included in these calculations, resulting in a higher degeneracy of bands.

The band dispersion of the supercell with $x = 1.89\%$ Sn resembles closely the pure Ge band structure, as well as the VCA band structure. This validates the unfolding procedure applied in the present work. The deduced direct band gap at the Γ point (E_g) and the indirect Γ-L band gap are summarized in Figs. 3(a) and 3(b) for the VCA and the supercell calculations, respectively. For a small Sn content [Fig. 2(a)], the direct and indirect alloy gaps compare well with the pure Ge gaps, which are without spin orbital coupling 0.97 and 0.82 eV, respectively. Disorder introduces a slight broadening of the peaks, but the standard deviation remains fairly small throughout the Brillouin zone.

With increasing Sn content, both gaps are reduced, and the alloy undergoes a transition from an indirect to a direct

semiconductor in the vicinity of $x = 4.85\%$. This transition, the band gaps, and the optical bowing parameters are the subjects of the following section. Before continuing, we note that the standard deviation increases as the Sn content increases, but not by much. This indicates that the QP particle peaks observed in experiments should remain fairly sharp even in the disordered alloy.

B. Indirect-direct gap transition and optical bowing

Both, the lowest direct and indirect gaps evaluated from the alloy band structures are plotted as function of the Sn content in Figs. 3(a) and 3(b). The results obtained by three approaches, the VCA [see Fig. 3(a)] and random supercells with and without relaxation of the atoms [see Fig. 3(b)], are compared. In Figs. 3(a) and 3(b), the insets show closeups of the regions where the Sn_xGe_{1-x} alloy transforms into a direct semiconductor. Again, the supercell calculations with relaxation are the reference to which the other calculations should be compared.

The VCA calculations were performed with and without SOC. As the Sn content increases, the effect of SOC increases from 100 meV for pure Ge to about 180 meV at 20% Sn. However, since SOC mainly raises the $J = 3/2$ states (VB1), this has very little effect on the point at which the transition from the indirect to a direct gap occurs. This is clearly highlighted by the inset in Fig. 3(a), which indicates that the critical Sn concentration changes by less than 0.5%, when SOC is included. Given the uncertainties of the present calculations, for instance the applied density functional, this effect can be safely disregarded. Therefore, we neglect SOC from here on.

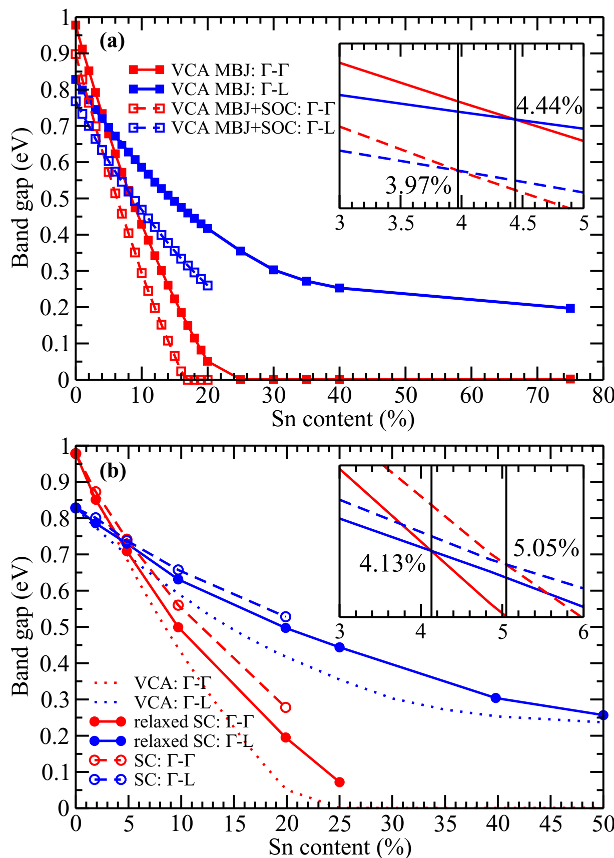

FIG. 3. (Color online) Sn_xGe_{1-x} alloy band gap as function of composition. The indirect Γ-L and direct Γ-Γ band gaps are given for a Sn content between $0 < x < 0.8$ calculated using the VCA (a) and unstrained random supercells (b) The supercells were either fully relaxed (solid circles) or only the volumes were optimized (open circles).

More critical is that the VCA and the supercell calculations show quite a different slope for the band gap. In the VCA the band gap is more quickly reduced than in the supercell calculations, as observed in Fig. 3(b). Neglecting the relaxation of the atomic positions in the supercell calculations enhances this effect even more. As a matter of fact, the relaxed supercell calculations take into account the effect of disorder and lattice relaxation correctly and should provide the best prediction for the experimental behavior.

Even though VCA and supercell calculations disagree on the slope, in both calculations the direct gap is more quickly reduced with increasing Sn content, resulting in an indirect-to-direct gap transition. The data extracted from the fully relaxed supercells yield this transition at a Sn content of 4.1% (compared to 4.4% for the VCA). In the supercell calculations, increasing the Sn content beyond 30% yields a semimetallic behavior for Sn_xGe_{1-x}. Since these calculations have neglected spin orbit coupling, and spin orbit coupling decreases the band gap by about 200 meV at 20% Sn, we expect that, experimentally, the insulator-to-metal transition should be rather observed around 20% Sn.

The indirect and direct band gaps deduced from the alloy band structures shown in Figs. 3(a) and 3(b) clearly exhibit a strongly nonlinear dependence on the Sn content. The deviation from linearity is often measured by the bowing parameter. For the evaluation of the optical bowing b_g the direct (Γ-Γ) gap dependence is fitted by a second-order polynomial of the form

$$\begin{aligned} E_g(x) &= xE_g[\text{Sn}] + (1-x)E_g[\text{Ge}] - b_g x(1-x) \\ &= x(E_g[\text{Sn}] - E_g[\text{Ge}] - b_g) + b_g x^2 + E_g[\text{Ge}]. \end{aligned} \quad (7)$$

As we can see in Fig. 3(a) such a fit is hardly sensible in the present case, as the nonlinearity is just way too strong. To be consistent with the experimental fitting procedure, we set $E_g[\text{Sn}]$ to -0.4 eV finding an optical bowing parameter $b_g = 3.1$ eV from the unstrained random supercells fitted to the composition range of $0 < x < 0.2$. The present fairly large optical bowing is in agreement with the experimental findings of He and Atwater [3] as well as D'Costa *et al.* [5]. The former studied Sn_xGe_{1-x} with $0 < x < 0.15$ by optical absorption measurements and proposed 2.8 eV. The latter directly observed the energy gaps employing spectroscopic ellipsometry and photoreflectance on Sn_xGe_{1-x} in the composition range $0.02 < x < 0.20$ at room as well as low temperature and proposed $b_g^{LT} = 2.61 \pm 0.10$ eV (strain corrected $b_g^{LT} = 2.26 \pm 0.09$ eV) and $b_g^{RT} = 1.94 \pm 0.10$ eV at low and room temperature, respectively. This significant temperature dependence of the bowing parameter was later experimentally confirmed by Pérez Ladrón de Guevara *et al.*, who observed $b_g^{RT} = 2.30 \pm 0.10$ eV and

$b_g^{LT} = 2.84 \pm 0.15$ eV [30]. More recently, Lin *et al.* deduced $b_g^{RT} = 2.42 \pm 0.04$ eV from photoreflectance [31], whereas room-temperature experiments from the same group yielded a somewhat lower value of $b_g^{RT} = 2.1 \pm 0.1$ eV 2 yr earlier [32]. However, it should be emphasized that the exceedingly strong nonlinearity of the gap makes a standard fitting of the optical bowing parameter pretty inaccurate: The direct gap changes by almost 0.7 eV over a range of 20%, with a remaining change of 0.6 eV over the residual 80% concentration change.

The indirect-to-direct gap transition and the optical bowing of the direct gap obtained by the random supercell approach are in reasonable agreement with the results of DFT calculations employing special quasirandom structures (SQSs) constructed from $2 \times 2 \times 2$ cubic cells containing 64 atoms with Sn concentrations of $x = 0.125$, 0.25, 0.50, and 0.75 [11]. These DFT calculations used the generalized gradient approximation for the XC potential. This approximation results in a negative band gap even for pure Ge, and this might make the predictions less reliable than the present calculations. The crossover from an indirect to a direct gap occurred at $x \sim 6.3\%$ and the bowing parameter b_g was ~2.8 eV. In a recent work by Gupta *et al.* [12], based on NL-EPM calculations, an optical bowing of 2.1–2.9 eV was predicted and the transition to a direct gap semiconductor occurred at $x = 6.5\%$ Sn content. However, to achieve agreement with experiment, a modified VCA with carefully chosen local and nonlocal parameters for the potential was used. Compared to these two calculations, the MBJLDA calculations presented here provide band structures and band gaps with higher accuracy than standard semilocal DFT and less empiricism than the NL-EPM calculations. We expect the present calculations to be more reliable than previous estimates. This is also supported by the observation that the indirect-to-direct gap transition is experimentally observed at a lower Sn content of $0.06 < x < 0.08$ in recent room-temperature photoluminescence experiments [32,33].

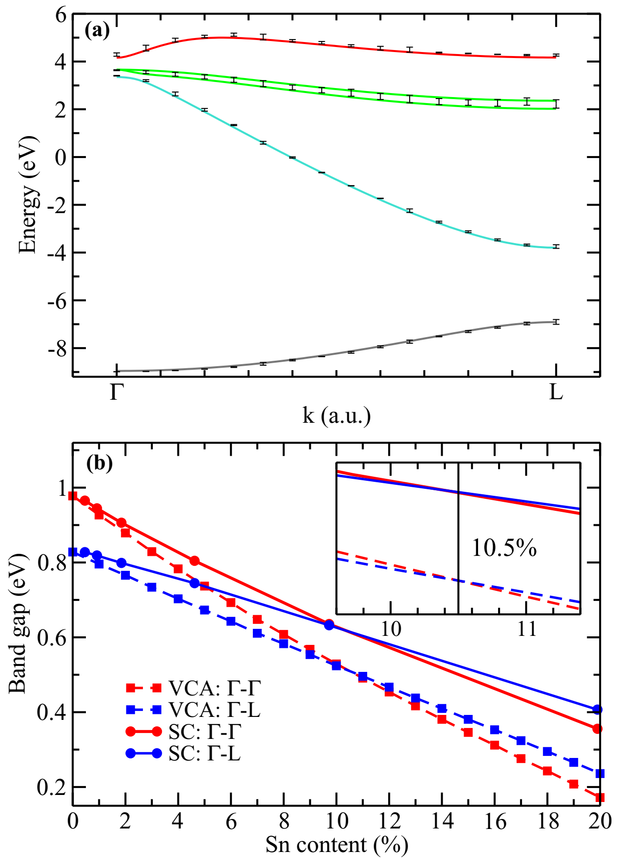

FIG. 4. (Color online) (a) Band structure of compressively strained Sn_xGe_{1-x} obtained by averaging over ten random supercells with Sn content of $x = 9.72\%$. The lattice constants $a = [100]$ and $b = [010]$ correspond to the Ge substrate lattice constant (5.644 Å), whereas the $c = [001]$ lattice constant was relaxed. The corresponding VCA band structure is shown by lines. Color coding is analogous to that of Fig. 2. (b) Direct Γ-Γ band gap (red) and the indirect Γ-L band gap (blue) as functions of Sn content obtained by VCA (squares), as well as the supercell approach (circles).

C. Laterally strained alloys

To realize Sn_xGe_{1-x} alloys, a common strategy is to grow the alloy on a suitably chosen substrate. In many cases, this growth is done epitaxially, implying that the in-plane lattice constant of the substrate is maintained. In order to study this case, we have performed VCA calculations for Sn_xGe_{1-x} alloys with the in-plane [100] and [010] lattice constants fixed to the LDA optimized Ge lattice constant (5.644 Å). In the third direction, $c = [001]$, the structures were fully relaxed. In Fig. 4(a) the band structure of laterally, compressively strained Sn_xGe_{1-x} with $x = 9.75\%$ is shown. In contrast to the unstrained case (Fig. 3), the VB1 state is split along Γ-L due to the strain, as indicated by the VCA band structure. In the supercell calculations it was difficult to separate those two subbands, since they partially overlap, when disorder is introduced. Instead we only show the mean value. The resulting mean deviation is large, and the bars indicating the standard deviation are roughly on top of the two bands found in the VCA.

The band gaps deduced from the strained random supercells are given in Fig. 4(b) as a function of the Sn content. Remarkably, the present calculations indicate that even under compressive strain a transition from an indirect to a direct gap semiconductor is predicted. Compressive strain in the [100] and [010] direction reduces the indirect gap more strongly than the direct gap (see below), and therefore works against the formation of a direct gap. In our calculation, this only delays the formation of a direct gap, which now occurs at a Sn concentration of roughly 10%. The VCA calculations again agree very well with the full supercell calculations, with the transition occurring also at roughly 10% Sn.

To study this in more detail, further calculations using the VCA were performed. The results of these calculations are presented in Fig. 5. The in-plane lattice constants $a = b = [100] = [010]$ were varied in the range of −3 to +4% compared to pure Ge (5.644 Å). Specifically, a "strain" of +3% corresponds to an increase of the in-plane lattice constant by 3% compared to bulk Ge, and that of −4% corresponds to a decrease of the in-plane lattice constant by 4% with respect to Ge. The 0% line corresponds to compressive strain on the Sn_xGe_{1-x} alloys, as the Sn_xGe_{1-x} alloy would rather adopt

a larger lattice constant than Ge. The cut at a strain of 0% has already been shown in Fig. 4(b). It is well accepted that tensile strain can produce a direct gap in Ge. Our calculations suggest this to occur at about 2% tensile strain for pure Ge consistent with the NL-EPM calculations of Gupta *et al.* [12], who suggested ∼1.5% tensile strain. Alternatively, a direct gap can be introduced by alloying with about 10% Sn, when the Sn_xGe_{1-x} is epitaxially grown on Ge. The trend that in-plane compressively strained Sn_xGe_{1-x} alloys exhibit the indirect-to-direct gap transition at higher Sn contents than the unstrained alloys was also experimentally observed [32]. The maps shown in Fig. 5 might help experimentalists to determine an optimal strategy for growing direct gap group IV Sn_xGe_{1-x} semiconductors.

IV. SUMMARY

We have computed the band structures and energy gaps of Sn_xGe_{1-x} using density-functional theory (DFT). Since standard density functionals underestimate the gap significantly, we have utilized the modified Becke-Johnson potential, which can be tuned to yield an excellent description of both the direct and the indirect band gap of Ge.

Two alternative approximations are used in the present work. The computationally more efficient method relies on the VCA: In this approach, every atom is replaced by two "virtual" atoms, one Sn and one Ge atom, and atomic "weights" consistent with the concentration x are assigned to the individual atoms. This approach is, in principle, elegant, but what has been often overlooked in literature is that it will only work if the potentials have been constructed with sufficient care: The combination of pseudopotentials and VCA only works if the pseudopotentials are designed to possess similar s and p pseudoorbitals for Sn and Ge. The potentials used in this work have been carefully designed to meet this criterion.

It is then not astonishing but still rather gratifying that the VCA results agree remarkably well with the computationally much more refined supercell calculations. In the present case, the supercell calculations were performed by simply placing Sn atoms randomly at Ge sites. Large supercells with 216 atoms were used, and the results were averaged over ten different random structures.

As previously observed, we find that the volumes of Sn_xGe_{1-x} alloys deviate significantly from Vegard's law. For intermediate Sn concentrations, the volume is larger than expected and the bowing parameter is about $b = -0.25$ Å. This is in good agreement with experiment.

For unstrained Sn_xGe_{1-x} alloys, the transition from an indirect to a direct gap semiconductor is calculated to occur around 4% Sn. The predicted transition concentration is mostly independent of the employed methods. Whether supercells or the VCA are used, whether spin orbit coupling is included or not, the results only vary by less than 0.5%.

Unfortunately the required Sn concentration increases to about 10%, when the Sn_xGe_{1-x} alloy is grown epitaxially on (100) Ge. As usual, the compressive strain exerted by the Ge substrate leads to a reduction of the indirect gap, partly counteracting the reduction of the direct gap by Sn alloying. Figure 5 is a central result of the present work. It maps out the indirect gap and the difference between the indirect and direct gap as a function of the Sn content and as a function of the in-plane [100] = [010] lattice constants of epitaxially grown Sn_xGe_{1-x} films. It might help to determine optimal growth strategies.

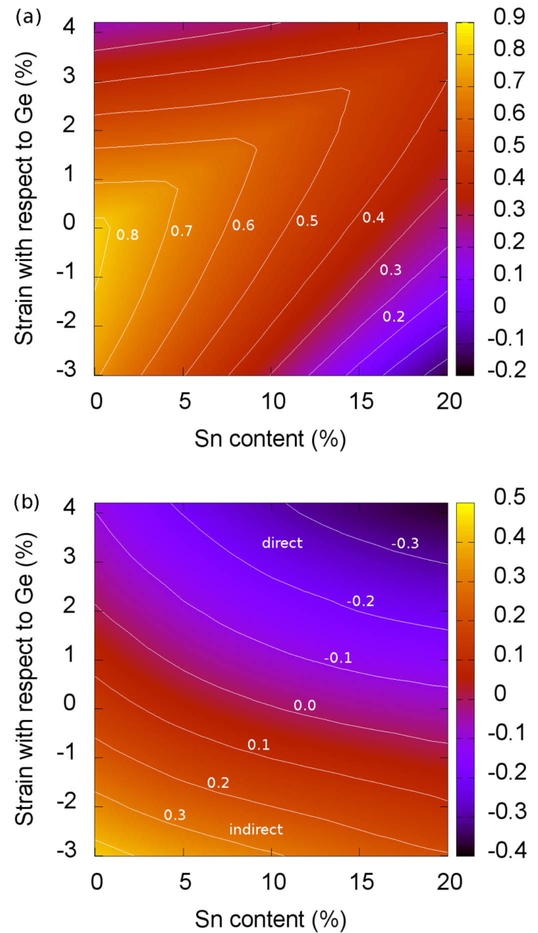

FIG. 5. (Color online) (a) Indirect gap of Sn_xGe_{1-x} in (eV) as a function of the Sn concentration x and the in-plane lattice constant ("strain"). The [100] and [010] lattice constants (a and b) are fixed, whereas the [001] lattice constant c was relaxed to minimize the total energy. A strain of 0% corresponds to the in-plane lattice constant of bulk Ge (5.644 Å). A strain of −3% implies an in-plane contraction of 3% compared to bulk Ge (compressive), whereas +4% corresponds to an in-plane lattice constant that is 4% larger than for bulk Ge. The calculations were performed using the VCA. (b) Difference between direct and indirect gap of Sn_xGe_{1-x}. Negative values correspond to a direct gap, positive values to an indirect gap. At 0% strain, the transition from an indirect to direct gap occurs at 10% Sn content [compare Fig. 4(b)].

ACKNOWLEDGMENTS

C.E. thanks T. Sander, J. Klimes, and the VASP team for their help and for useful discussions as well as the Vienna Scientific Cluster team for the support in running the VASP code. The calculations were performed at the Vienna Scientific Cluster. This work was partly funded by the special research program IR-ON of the Austrian Science Fund.

[1] F. Zhang, V. H. Crespi, and P. Zhang, Phys. Rev. Lett. **102**, 156401 (2009).
[2] M. V. Fischetti and S. E. Laux, J. Appl. Phys. **80**, 2234 (1996).
[3] G. He and H. A. Atwater, Phys. Rev. Lett. **79**, 1937 (1997).
[4] K. A. Mäder, A. Baldereschi, and H. von Känel, Solid State Commun. **69**, 1123 (1989).
[5] V. R. D'Costa, C. S. Cook, A. G. Birdwell, C. L. Littler, M. Canonico, S. Zollner, J. Kouvetakis, and J. Menéndez, Phys. Rev. B **73**, 125207 (2006).
[6] M. Bauer, J. Taraci, J. Tolle, A. V. G. Chizmeshya, and S. Zollner, Appl. Phys. Lett. **81**, 2992 (2002).
[7] J. Mathews, R. T. Beeler, J. Tolle, C. Xu, R. Roucka, J. Kouvetakis, and J. Menéndez, Appl. Phys. Lett. **97**, 221912 (2010).
[8] T. C. Chiang and F. J. Himpsel in *Landolt-Börnstein—Group III Condensed Matter*, edited by A. Goldmann and E.-E. Koch (Springer-Verlag, Berlin, Heidelberg, New York, 1989), Vol. 23a.
[9] L. Vegard, Z. Phys. **5**, 17 (1921); A. R. Denton and N. W. Ashcroft, Phys. Rev. A **43**, 3161 (1991).
[10] H. Pérez Ladrón de Guevara, A. G. Rodríguez, H. Navarro-Contreras, and M. A. Vidal, Appl. Phys. Lett. **84**, 4532 (2004).
[11] W.-J. Yin, X.-G. Gong, and S.-H. Wei, Phys. Rev. B **78**, 161203 (2008).
[12] S. Gupta, B. Magyari-Köpe, Y. Nishi, and K. C. Saraswat, J. Appl. Phys. **113**, 073707 (2013).
[13] P. Hohenberg and W. Kohn, Phys. Rev. **136**, B864 (1964).
[14] W. Kohn and L. J. Sham, Phys. Rev. **140**, A1133 (1965).
[15] G. Kresse and J. Furthmüller, Phys. Rev. B **54**, 11169 (1996).
[16] P. E. Blöchl, Phys. Rev. B **50**, 17953 (1994); G. Kresse and D. Joubert, *ibid.* **59**, 1758 (1999).
[17] D. M. Ceperley and B. J. Alder, Phys. Rev. Lett. **45**, 566 (1980).
[18] J. P. Perdew, K. Burke, and M. Ernzerhof, Phys. Rev. Lett. **77**, 3865 (1998).
[19] J. P. Perdew, A. Ruzsinszky, G. I. Csonka, O. A. Vydrov, G. E. Scuseria, L. A. Constantin, X. Zhou, and K. Burke, Phys. Rev. Lett. **100**, 136406 (2008).
[20] K. Hummer, J. Harl, and G. Kresse, Phys. Rev. B **80**, 115205 (2009).
[21] F. Tran and P. Blaha, Phys. Rev. Lett. **102**, 226401 (2009).
[22] Y.-S. Kim M. Marsman, G. Kresse, F. Tran, and P. Blaha, Phys. Rev. B. **82**, 205212 (2010).
[23] C. I. Ventura, J. D. Fuhr, and R. A. Barrio, Phys. Rev. B **79**, 155202 (2009).
[24] L. Bellaiche and D. Vanderbilt, Phys. Rev. B **61**, 7877 (2000).
[25] F. F. Murnaghan, Proc. Natl. Acad. Sci. USA **30**, 244 (1944).
[26] V. Popescu and A. Zunger, Phys. Rev. Lett. **104**, 236403 (2010).
[27] V. Popescu and A. Zunger, Phys. Rev. B **85**, 085201 (2012).
[28] H. Pérez Ladrón de Guevara, A. G. Rodríguez, H. Navarro-Contreras, and M. A. Vidal, Appl. Phys. Lett. **83**, 4942 (2003).
[29] Y. Chibane and M. Ferhat, J. Appl. Phys. **107**, 053512 (2010).
[30] H. Pérez Ladrón de Guevara, A. G. Rodríguez, H. Navarro-Contreras, and M. A. Vidal, Appl. Phys. Lett. **91**, 161909 (2007).
[31] H. Lin, R. Chen, W. Lu, Y. Huo, T. I. Kamins, and J. S. Harris, Appl. Phys. Lett. **100**, 102109 (2012).
[32] R. Chen, H. Lin, Y. Huo, C. Hitzman, T. I. Kamins, and J. S. Harris, Appl. Phys. Lett. **99**, 181125 (2011).
[33] G. Grzybowski, R. T. Beeler, L. Jiang, D. J. Smith, J. Kouvetakis, and J. Menéndez, Appl. Phys. Lett. **101**, 072105 (2012).